The Convection, Aerosol, and Synoptic-Effects in the Tropics (CAST) Experiment

Building an Understanding of Multiscale Impacts on Caribbean Weather via Field Campaigns

N. Hosannah, J. González, R. Rodriguez-Solis, H. Parsiani, F. Moshary, L. Aponte, R. Armstrong, E. Harmsen, P. Ramamurthy, M. Angeles, L. León, N. Ramírez, D. Niyogi, and B. Bornstein

CARIBBEAN RAINFALL MODES. The Caribbean basin (8°–22°N, 85°–60°W) is a complex region in which an understanding of the factors affecting water availability and associated rainfall production is important for the survival of millions of people and for the protection of sensitive ecosystems. Precipitation in the Caribbean is bimodal, with average peaks in the early (April–July) and late (August–November) rainfall seasons (averages of 216 and 178 mm month^{-1}, respectively), while June–July is a drier period within the early rainfall season (average of 114 mm month^{-1}) known as the midsummer drought. The dry season spans from December to March and, generally, exhibits lower rainfall totals (averages between 12 and 60 mm month^{-1}).

Large-scale phenomena such as El Niño–Southern Oscillation (ENSO) and the North Atlantic Oscillation (NAO; with its associated North Atlantic high pressure) modify sea surface temperatures (SSTs) and precipitable water in the Caribbean. SSTs are coupled with winds via changes in atmospheric stability that accompany ENSO and NAO variations, and increases in water temperatures that enhance air buoyancy, thus reducing vertical wind shear and promoting thermal convection. These wind–evaporation–SST feedbacks work down to local island scales to govern spatiotemporal moisture and rainfall patterns. An additional impactful element is Saharan dust that is transported across the Atlantic Ocean via the trade winds in a dry-air layer originating over North Africa. The dust transport is observed mostly during the summer months, with dust event intensity and frequency peaking in July. Dust events affect weather through their association with dry, warm air masses and also by impacting cloud-scale microphysical processes via the suppression of cloud droplet growth mechanisms.

Although large-scale phenomena regulate spatiotemporal precipitation patterns in the Caribbean, the region's island-scale rainfall is also influenced by local convective processes modified by topography, land cover, soil moisture, and proximity to coastal waters. For example, the Puerto Rican Cordillera Central is a large east–west-oriented mountain range along the island's central axis, with several peaks above 1 km (Fig. 1), the highest of which is Cerro de Punta at 1.34 km; the El Yunque natural rain forest is on the slopes of the highest peak on the eastern side of the island, at 1.07 km. These elevated sites induce orographic precipitation when moist air is forced upward over them. Another location-dependent process occurs at the western edge of the island where the easterly trade winds converge with westerly sea breezes caused by surface heating, inducing or intensifying afternoon convective storms. These processes are further modified by changes in

AFFILIATIONS: Hosannah, González, Moshary, Ramamurthy, and Angeles—City College of New York, New York, New York; Rodriguez-Solis, Parsiani, Aponte, Armstrong, Harmsen, León, and Ramírez—University of Puerto Rico at Mayaguez, Mayaguez, Puerto Rico; Niyogi—Purdue University, West Lafayette, Indiana; Bornstein—San Jose State University, San Jose, California
CORRESPONDING AUTHOR: Nathan Hosannah, nhosannah@gmail.com

DOI:10.1175/BAMS-D-16-0192.1

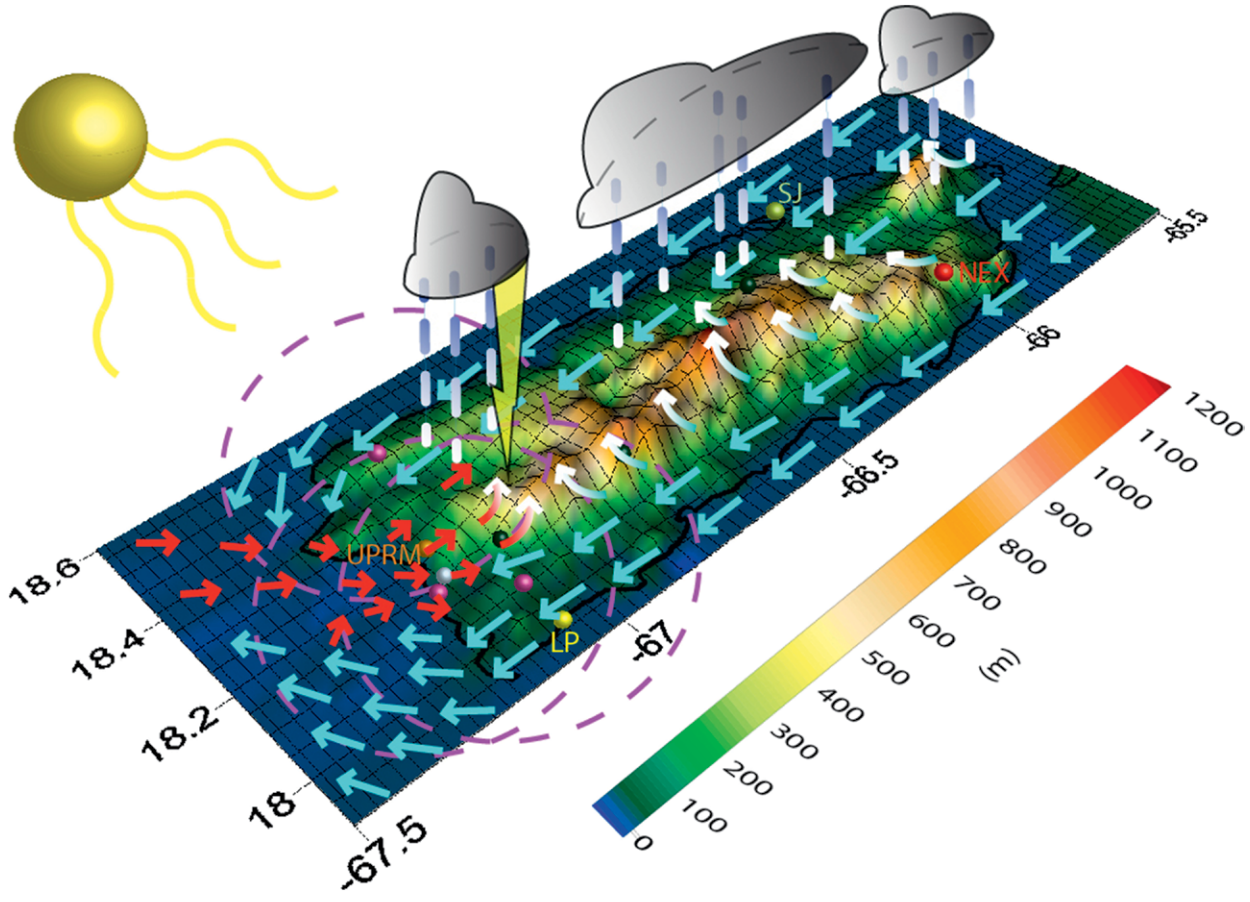

Fig. 1. Topographic map of Puerto Rico (m; shaded) showing local processes, including surface heating, orography (red–white and blue–white arrows lifting up mountains), and convergence between sea-breeze (red arrows) and easterly (blue arrows) winds. Sensor sites are also shown, including the NWS NEXRAD site (NEX), Tropinet radar sites (purple dots) and ranges (purple dashes), the UPRM site (UPRM), the La Parguera site (LP), San Juan (SJ), NRCS soil moisture sites (black dots), and the Cabo Rojo soil moisture site (silver dot).

land cover and soil moisture, which impact sensible and latent heat fluxes.

To better understand how island-scale processes contribute to regional-scale Caribbean precipitation, improved monitoring in the Caribbean islands must be considered. Currently, there are too few observational sensors for in-depth analyses of island-scale rainfall patterns, as well as of local surface and atmospheric conditions. One exception is Puerto Rico, with its extensive network of ground-based and in situ sensors.

GAPS IN THE PUERTO RICO OBSERVATIONAL NETWORK. Puerto Rico has over 40 active U.S. Geological Survey surface stations that measure precipitation, eight Natural Resource Conservation Service (NRCS) soil moisture sensor sites, a Next Generation Weather Radar (NEXRAD) site, three Aerosol Robotic Network (AERONET) sunphotometers, and twice-daily National Weather Service (NWS) radiosonde launches at 0000 (2000) and 1200 (0800) UTC [Atlantic standard time (AST)]. Since most of these instruments are located on, or deployed from, the eastern side of the island, additional ground and in situ sensors are necessary to properly monitor convective storm dynamics on the western side. The necessity to improve observational capabilities and to better understand local convective processes using western observations led to the Convection, Aerosol, and Synoptic-Effects in the Tropics (CAST) campaign.

CAST INSTRUMENTATION AND PROTOCOLS. CAST was conducted by researchers from multiple institutions including the University

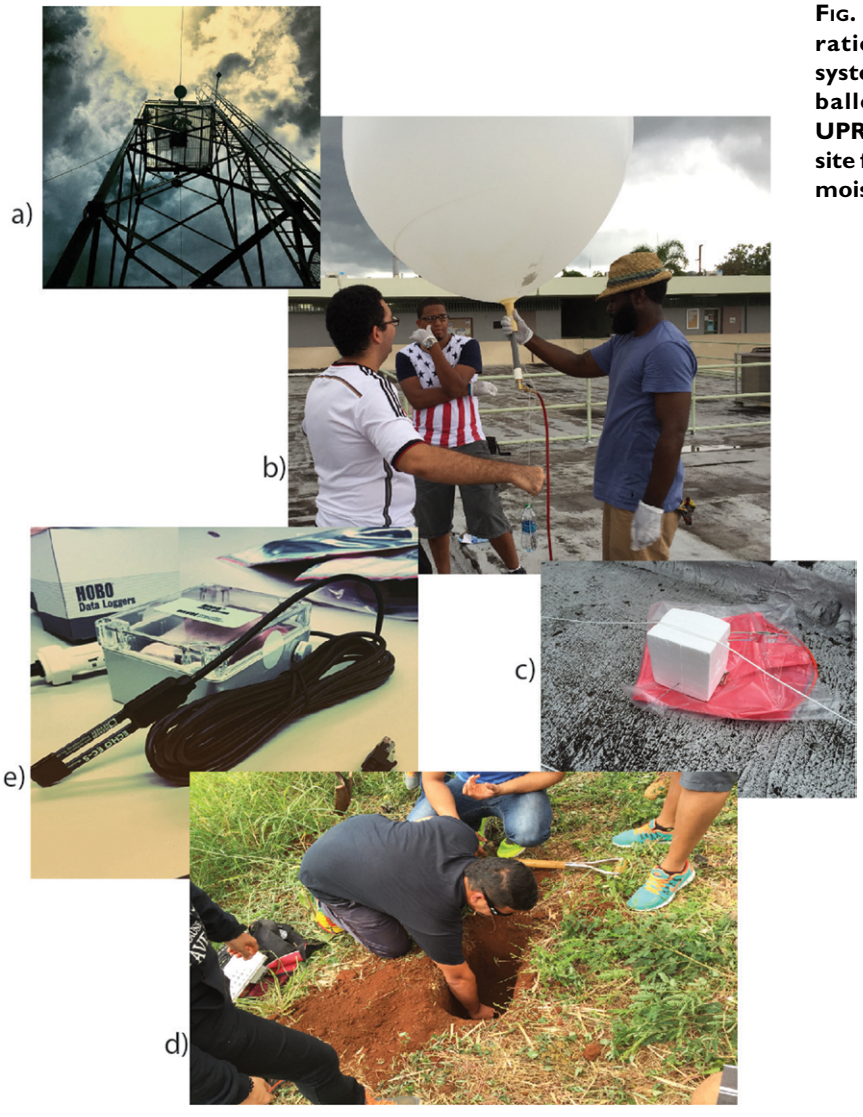

Fig. 2. Instruments and field study preparations: (a) Cabo Rojo Tropinet radar system, (b) preparation for a radiosonde balloon launch, (c) radiosonde atop a UPRM building, (d) readying the Mayaguez site for soil moisture sensors, and (e) a soil moisture sensor.

of Puerto Rico at Mayaguez (UPRM), City College of New York (CCNY), NWS in San Juan, Purdue University (PU), and San Jose State University (SJSU) (Fig. 2). Three CAST phases were scheduled to monitor atmospheric conditions in western Puerto Rico during three of its distinct seasons including the midsummer drought (phase I, 22 June–10 July 2015), the dry season (phase II, 6–22 February 2016), and the early rainfall season (phase III, 24 April–7 May 2016). A phase summary is shown in Table 1.

Supplemental CAST instrumentation included up to twice-daily radiosonde launches, three high-resolution radars, a ceilometer, a disdrometer, soil moisture sensors, and an aerosol speciation sampler, all on the western side of the island. Instrumented locations (Fig. 1) included UPRM (18.21°N, 67.14°W), fitted with a CL51 ceilometer (Vaisala), a Cimel Electronique 318A spectral radiometer (AERONET), a disdrometer, and nearby Echo EC-5 soil moisture sensors at multiple depths (0.05, 0.1, 0.2, 0.5, and 1 m). These soil moisture sensors were placed at the same latitude (18.15°N)

Table 1. CAST phase log.

Phase (time period)	No. of days with max rain > 40 mm	No. of days with sea breeze	Background flow	No. of days with orographic effects	No. of days with AOT (1020 nm) > 0.2	1300 AST relative humidity (%)
I (22 Jun–10 Jul 2015)	5/19	9/19	E to ENE	4/19	12/19	75–88
II (6–22 Feb 2016)	12/17	8/17	S to NNE	6/17	0/17	52–89
III (24 Apr–7 May 2016)	10/14	1/14	S to ENE	2/14	2/14	73–90

as two western NRCS sites [Maricao (18.15°N, 67°W) and Guilarte (18.15°N, 66.77°W)] for comparative purposes. The disdrometer, soil moisture sensors, and ceilometer ran continuously. M10 radiosondes (Meteomodem) were launched from the roof of one of the UPRM buildings. The La Parguera (17.98°N, 67.04°W) site had an AERONET radiometer and an air sampler. Each of the three short-range dual-polarized X-band Doppler radars at Cabo Rojo (18.16°N, 67.18°W), Lajas (18.03°N, 67.08°W), and Isabela (18.06°N, 67.05°W) could scan vertically or spatially and were implemented only when western storms occurred.

All instruments were checked and calibrated before each phase. Researchers communicated daily to synchronize efforts. To ensure optimal radiosonde launch times, NWS forecasts and weather maps, along with aerosol optical thickness (AOT) forecasts from the National Aeronautics and Space Administration (NASA) Goddard Earth Observing System (GEOS-5) model, were analyzed to ensure that a range of conditions including low and high AOT for dry and wet days were sampled. During phase I, 12 radiosonde launches were carried out over a 3-week period. While phases II and III were each a week shorter, they each had more launches than phase I—an average of two daily, during weekdays. Efforts were made to launch up to 30 min before forecasted storms and just after completion of afternoon or evening showers when possible during the two 2016 phases.

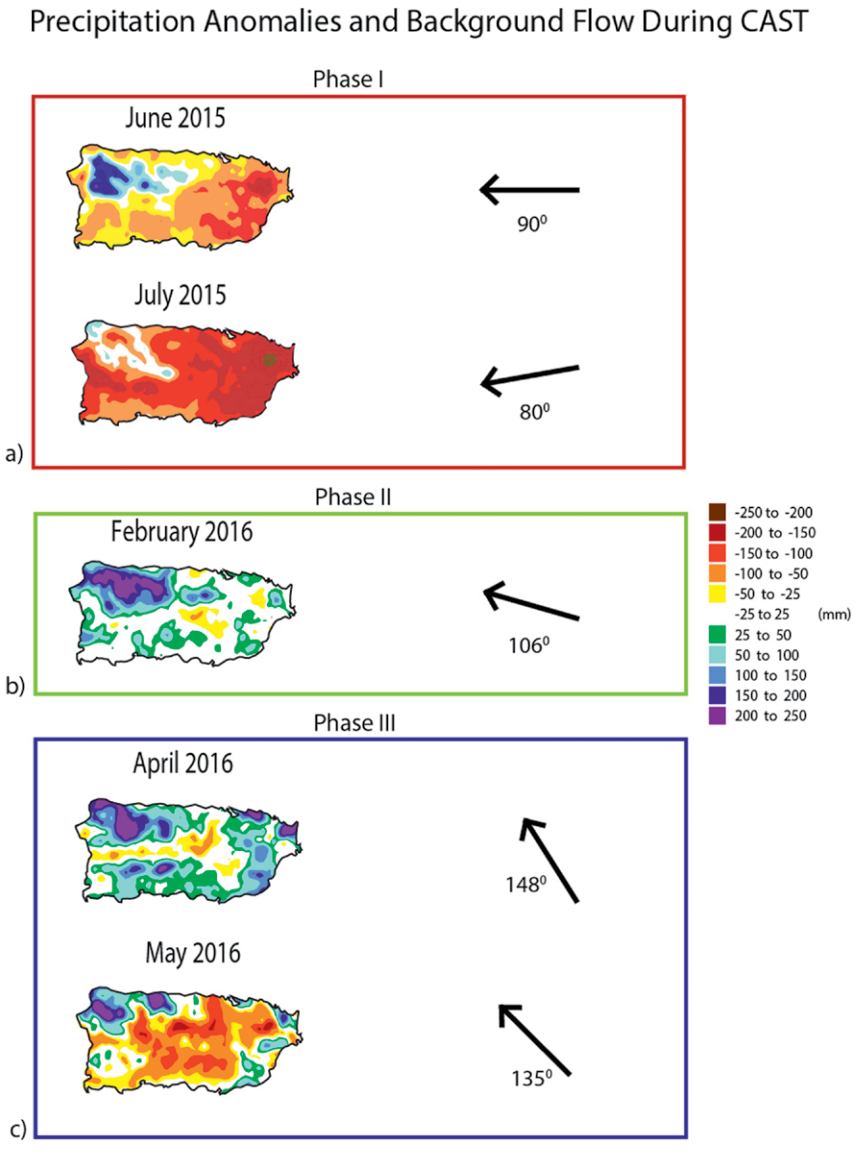

Fig. 3. Advanced Hydrologic Prediction Service (AHPS) total precipitation monthly climatological anomalies (mm; shaded) and prevailing background flow direction (arrows) for CAST phases (a) I, (b) II, and (c) III.

CONDITIONS DURING CAST. Phase I (22 June–10 July 2015) was conducted during the extreme Caribbean summer drought of 2015, which occurred during a strong El Niño and a positive NAO phase. The drought caused island-wide emergency water management practices in Puerto Rico, including water rationing and potable water distribution. Precipitable water from the National Centers for Environmental Prediction (NCEP) reanalysis dataset (and corroborated by satellite imagery) revealed negative anomalies in the Caribbean (3–4 kg m^{-2}, or 4%–6% less than climatological averages), which along with cooler SSTs attained from the Optimum Interpolated Sea Surface Temperature (OISST) product (0.2°–1°C less than the 27.5°C climatological value) could possibly mitigate rain production. Furthermore, frequent intense dust events occurred during phase I,

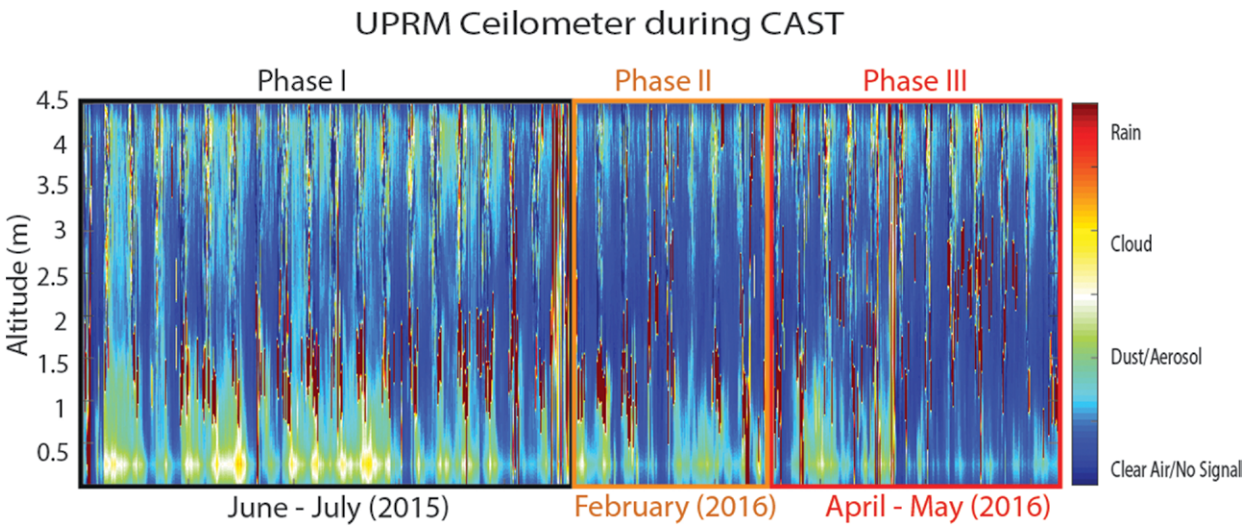

Fig. 4. Ceilometer 910-nm backscatter for CAST phases I (black rectangle), II (orange rectangle), and III (red rectangle).

and the regional 550-nm aerosol optical depth (AOD) average from the Moderate Resolution Imaging Spectroradiometer (MODIS) product was higher than usual, a value of 0.36 compared with the 14-yr-average value of 0.3 (2003–16). In addition, ENSO was determined via the multivariate ENSO index (MEI) to be a warm event (two standard deviations above normal); meanwhile, the drought strength determined from the standard precipitation index (SPI) was three standard deviations below normal. These numbers are indicative of extremely dry Caribbean conditions and are reflected in the reduced rain days over Puerto Rico, although maximum daily rain accumulations above 40 mm occurred over the island on 27% of phase I campaign days. Precipitation anomalies from the Advanced Hydrologic Prediction Service (Fig. 3a) showed drier-than-normal conditions for more than 70% of the island in June by −25 mm or more, and for more than 85% of the island during July by −50 mm or more. Positive precipitation anomalies greater than 50 mm, however, occurred in June over the northwest quadrant, more than 20% of the island, and may be indicative of locally enhanced precipitation.

During the dry season (phase II, 6–22 February 2016), positive precipitable water anomalies (8%, 38 kg m^{-2}) were found over western Puerto Rico and the Lesser Antilles, while negative anomalies (6%, 33 kg m^{-2}) were detected toward the central and southwestern Caribbean Sea. Despite SSTs near annual lows, values were warmer than February climatological values by 0.3°–1°C (26.5°C seasonal average). Moreover, dust content was low, with an AOD average of 0.19, normal for February. Locally over Puerto Rico, rain exceeding 40 mm fell on 70% of days, with positive rainfall anomalies above 50 mm in the northwest and in pockets along the west, southeast, and south-central coasts, as well as El Yunque (Fig. 3b).

SSTs during the early rainfall season (phase III, 24 April–7 May 2016) were unseasonably high by 0.4°–1.0°C, approximately 28°C in the Caribbean Sea. Furthermore, precipitable water anomalies of 6%–10% (42–44 kg m^{-2}) were detected along with lower-than-normal AOD, 0.23 as compared with the 14-yr MODIS average of 0.26. Positive April rainfall anomalies above 50 mm in Puerto Rico occurred along all but the western coasts (Fig. 3c), with negative anomalies of 50–100 mm along the Cordillera mountain range. However, trends changed during May with negative precipitation anomalies exceeding 50 mm at the center, southern coast, and northeast quadrant. Phase III was the wettest of the three periods, with maximum rain totals above 40 mm on 71% of days, an expected result considering the warmer SSTs, positive precipitable water anomalies, and low dust during this time frame.

CAST DATA. The ceilometer 910-nm backscatter aerosol signature varies diurnally and seasonally (Fig. 4), showing maximum intensity between the surface and 4 km during phase I and decreased intensity during phases II and III, most notably between the surface and 0.5 km. Column-integrated AOT from AERONET (not shown) yields 1640-nm average large-particle AOT values of 0.256, 0.066,

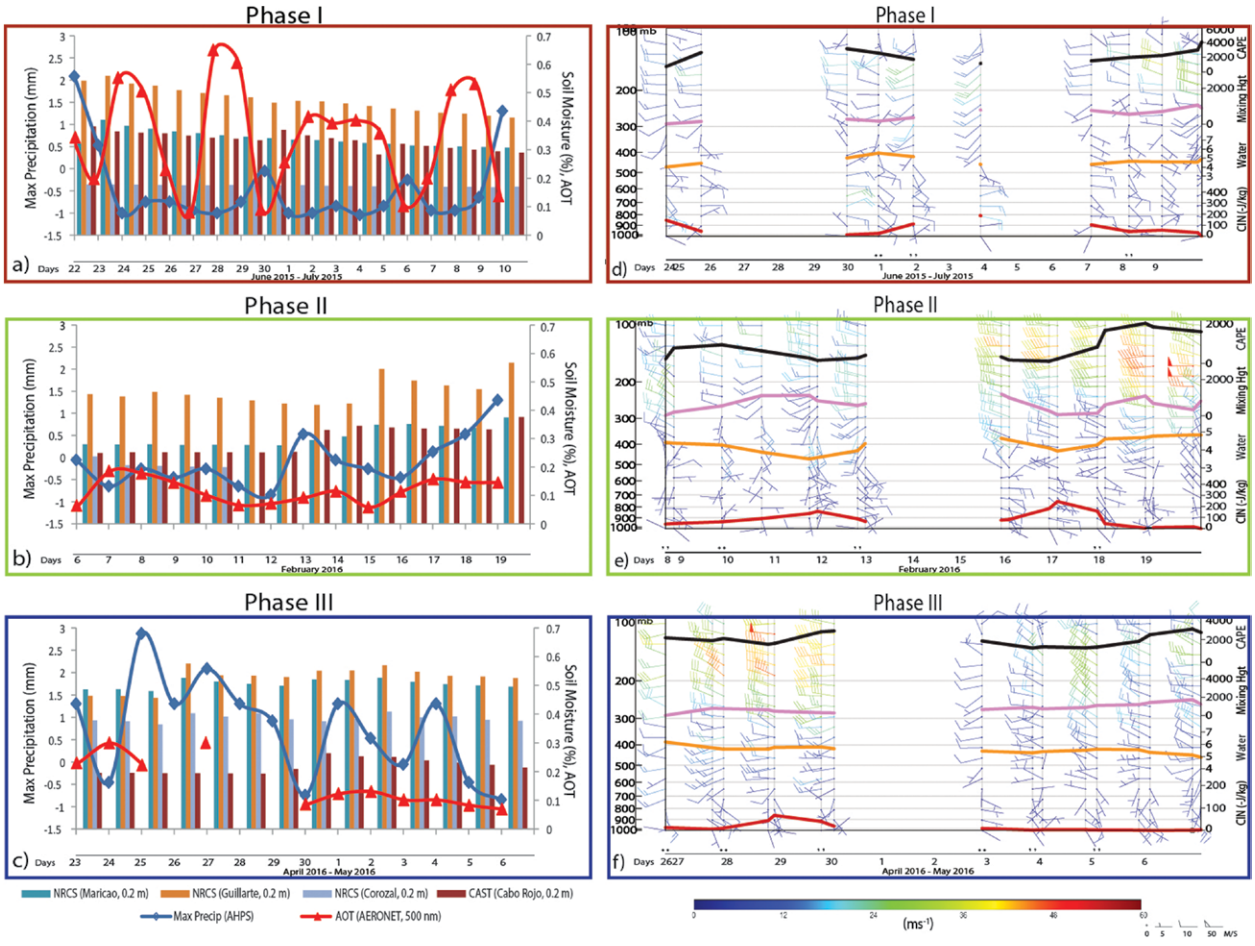

Fig. 5. AHPS normalized maximum precipitation (blue line), 500-nm AERONET AOT (red line), and 0.2-m-depth soil moisture for NRCS Maricao (aqua bars), Guillarte (orange bars), Corozal (light blue bars), and CAST Cabo Rojo (brown bars) during CAST phases (a) I, (b) II, and (c) III. In addition, radiosonde data are shown for phase I: (d) horizontal wind (barbs), convective available potential energy (CAPE; J kg^{-1}, black line), CIN (J kg^{-1}; red line), precipitable water (kg m^{-2}; orange line), and mixing height (m; pink line). (e),(f), As in (d), but for phases II and III, respectively.

and 0.074 for phases I–III, respectively; while 500-nm (medium particle) values are 0.342, 0.107, and 0.130, respectively; and 340-nm (small particle) averages are 0.348, 0.123, and 0.250, respectively, exhibiting a nearly fourfold increase in large-wavelength (large particle) AOT when comparing phase I to phases II and III. The soil moisture 0.2 m below the surface, maximum precipitation, and 500-nm AOT for each phase are presented in Figs. 5a–c. Phases I and II show wetter soil conditions at western sites (Cabo Rojo, Maricao, and Guillarte) than farther east (Corozal, 18.32°N, 66.36°W), while the soil moisture in the east increases during phase III.

Composites of all the radiosonde launches for each phase (Figs. 5d–f) show higher CAPE during phases I and III than during phase II. Lower wind speeds (at levels >700 hPa) are observed during phase I (Fig. 5d) as compared with phases II and III (Figs. 5e,f). Local precipitable water values during phases I and III are higher than in phase II by an average of approximately 0.01 m. The dry season (phase II) also exhibits the lowest convective inhibition (CIN) values of all three phases, and mixing heights (0–1.5 km) between the minima produced in phase I (0–1 km) and the maxima produced in phase III (0–2 km). Dewpoint depressions (not shown) between 800 and 400 hPa were highest (>50°C) during nonrain days in phase II, as compared to phases I and III, with averages of 35° and 20°C, respectively. In the following section, we focus on one CAST event via the presentation of campaign data.

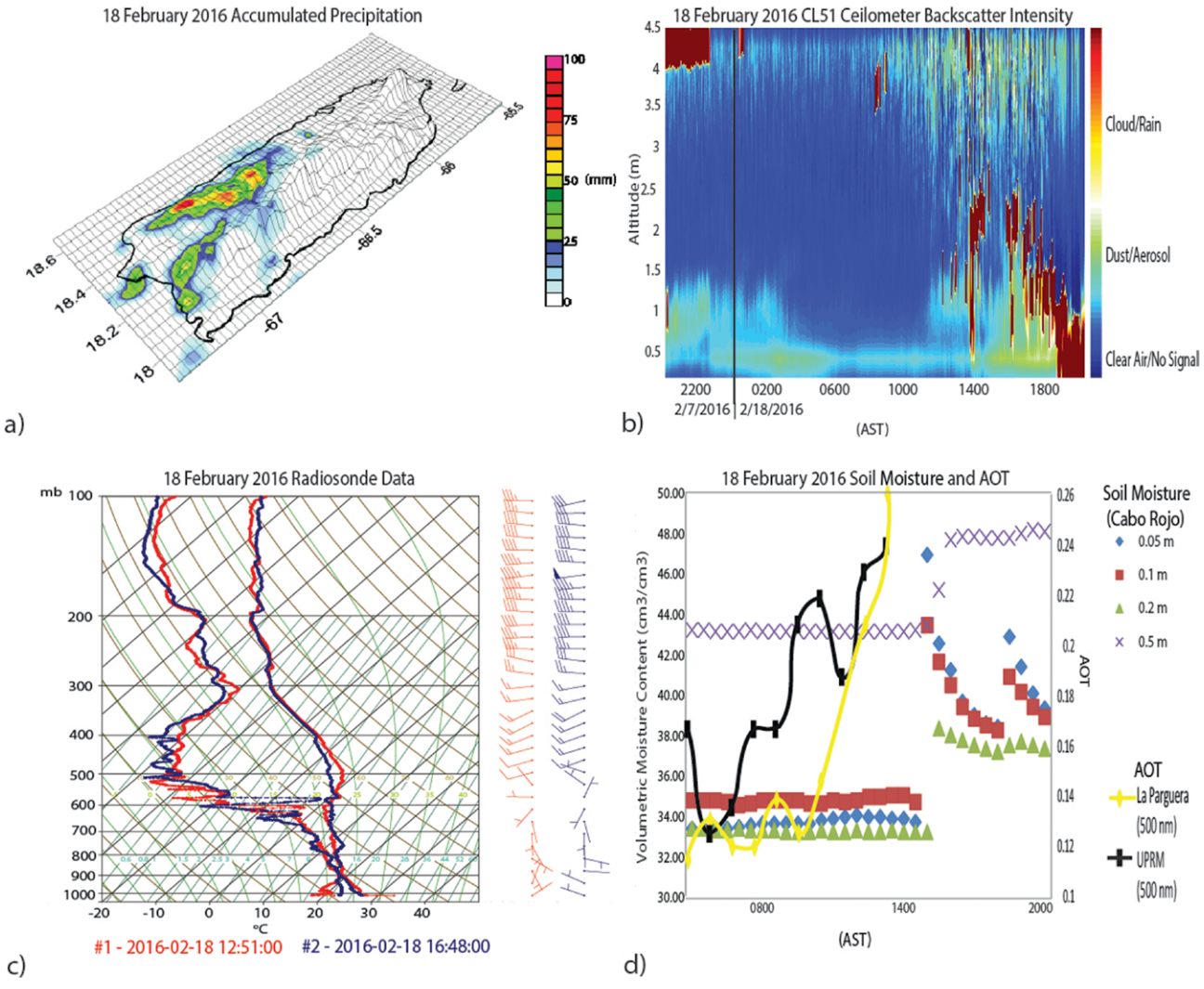

Fig. 6. Data for the 18 Feb 2016 storm. (a) AHPS total accumulated precipitation, (b) CL51 backscatter intensity, (c) radiosonde data (left lines are dewpoint temperature plots; right lines are ambient temperature plots) at 1251 (red lines) and 1648 (blue lines) AST, and (d) Cabo Rojo soil moisture content and 500-nm AERONET AOT results at UPRM and La Parguera.

A CAST CASE STUDY. To illustrate the value of CAST data, we present a large storm that took place over western Puerto Rico on 18 February 2016 as a case study. The rain event occurred as a mid- to upper-level ridge eroded, and a polar trough shifted into the central Atlantic. The intense rainfall yielded rain accumulations of 50 mm or more in a period of 12 h, mostly over the northwestern and western slopes of the Cordillera Central (Fig. 6a). Ceilometer data (Fig. 6b) show moderate backscatter intensity prior to the beginning of the rainfall at UPRM (1845 AST), and cloud heights ranging from as low as 0.5 km to beyond 4 km (the instrument detection limit is 4.5 km). A skew-*T* diagram of the 1251 and 1648 AST radiosonde launches (Fig. 6c) shows cloud levels as high as 600 hPa, land surface temperatures at ~28°C, and evidence of westerly sea-breeze strengthening from the early to late afternoon hours. In addition, the environment became more humid from the early to late afternoon. AERONET 500-nm AOT values (Fig. 6d) at La Parguera and UPRM ranged from 0.11 to 0.25, high compared to the phase II average (0.107). Soil moisture at the Cabo Rojo site (also Fig. 6d) was nearly constant until 1745 AST, when it increased 5–13 cm^3 cm^{-3} from the surface to the 0.5-m depth in response to the rainfall.

The CAST data point, at the very least, to localized enhancement of this rain event as a result of topography and strong sea-breeze influences (revisiting the convection process diagram in Fig. 1), although further study is necessary to determine the individual contributions of these factors in convection enhancement and to explore their interplay with the leading large-scale conditions.

CLOSING REMARKS. CAST observations have provided pertinent information about atmospheric conditions in western Puerto Rico during three of the island's distinct seasons, providing a starting point for the analysis of convective interplay in the coastal tropics. The results reported herein are only a first step in furthering our understanding of the interconnectedness of multiscale precipitation drivers in tropical coastal environments to support the overall long-term goal of improving weather prediction in sensitive and complex regions such as the Caribbean.

Future CAST phases will allow for additional cross-seasonal comparisons and analysis. CAST also provides a basis for setting up modeling experiments centered around some of the more extreme convective events occurring during the experiment. The incorporation of a cloud-resolving model will allow us to further investigate multiscale interactions between large- and local-scale processes and zoom in on their effects on island convection and precipitation. CAST data, event descriptions, and synthesis reports to date may be accessed at the CCNY Coastal Urban Environmental Research Group website (http://cuerg.ccny.cuny.edu/).

ACKNOWLEDGMENTS. Thanks to NSFAGS-1433430, DOEd P031M105066, and NOAA-CREST (NA17AE1625) for their support and AERONET, NRCS, NCEP, and NOAA for data used herein. Special thanks to V. Morris, W. Peña, C. Lunger, J. Diaz, D. Gonzalez, and R. Davis.

FOR FURTHER READING

Angeles, M. E., J. E. González, N. D. Ramírez-Beltrán, C. A. Tepley, and D. E. Comarazamy, 2010: Origins of the Caribbean rainfall bimodal behavior. *J. Geophys. Res.,* **115,** D11106, doi:10.1029/2009JD012990.

Carlson, T. N., and J. M. Prospero, 1972: The large-scale movement of Saharan air outbreaks over the northern equatorial Atlantic. J. Appl. Meteor., 11, 283–297, doi:10.1175/1520-0450(1972)011<0283:TLSMOS>2.0.CO;2.

Gamble, D. W., and S. Curtis, 2008: Caribbean precipitation: Review, model, and prospects. *Prog. Phys. Geogr.,* **32,** 265–276, doi:10.1177/0309133308096027.

Hosannah, N., H. Parsiani, and J. E. González, 2015: The role of aerosols in convective processes during the midsummer drought in the Caribbean. *Adv. Meteor.,* **2015,** 261239, doi:10.1155/2015/261239.

Jury, M. R., S. Chiao, and E. W. Harmsen, 2009: Mesoscale structure of trade wind convection over Puerto Rico: Composite observations and numerical simulation. *Bound.-Layer Meteor.,* **132,** 289–314, doi:10.1007/s10546-009-9393-3.

Keyantash, J. and J.A. Dracup, 2002: The quantification of drought: An evaluation of drought indices. *Bull. Amer. Meteor. Soc.,* **83,** 1167–1180, doi:10.1175/1520-0477(2002)083<1191:TQODAE>2.3.CO;2.

Rosenfeld, D., Y. Rudich, and R. Lahav, 2001: Desert dust suppressing precipitation: A possible desertification feedback loop. *Proc. Natl. Acad. Sci. USA,* **98,** 5975–5980, doi:10.1073/pnas.101122798.

Wolter, K., and M. S. Timlin, 2011: El Niño/Southern Oscillation behaviour since 1871 as diagnosed in an extended multivariate ENSO index (MEI.ext). *Int. J. Climatol.,* **31,** 1074–1087, doi:10.1002/joc.2336.